# Molecular dynamics study of structural properties of amorphous $Al_2O_3$

Gonzalo Gutiérrez*
*Departamento de Física, Universidad de Santiago, Casilla 307, Santiago 2, Chile*

Börje Johansson†
*Condensed Matter Theory Group, Department of Physics, Uppsala University, Box 530, S-751 21, Uppsala, Sweden*
(Received 8 August 2001; published 11 February 2002)

The structural properties of amorphous aluminum oxide ($Al_2O_3$) have been investigated by means of the molecular dynamics technique. The simulations were done in a microcanonical ensemble, using a pairwise potential, on systems with up to 1800 particles. Three different systems, at densities ranging from 3.0 to 3.3 g/cm$^3$, were prepared by quenching from the melt. The network topology of our system is analyzed through partial pair correlations, coordination numbers, angle distributions, and ring statistics. A detailed analysis of the interatomic distances reveals that in the amorphous state there is a short-range order dominated by a slightly distorted $(AlO_4)^{5-}$ tetrahedron, in agreement with recent experimental results. This conclusion is supported by the distribution of nearest-neighbor coordination numbers, where more than 75% of Al atoms have four O as nearest-neighbors. Ring statistics reveal the presence of two- to fivefold rings, with a peak at the fourfold ring and where the two- and threefold rings are planar. Comparison with available experimental data and earlier calculations shows that the structures of amorphous and liquid alumina are very similar. The amorphous structure also presents close similarities to the surface structure of $\gamma$-alumina at room temperature. Simulations for systems at different densities show that the coordination number of the elementary unit increases as the density increases, suggesting that the tetrahedrally and octahedrally coordinated forms of amorphous alumina found experimentally correspond to different densities.

DOI: 10.1103/PhysRevB.65.104202 PACS number(s): 61.43.Fs, 81.05.Pj

## I. INTRODUCTION

Amorphous alumina is of great interest both from the experimental and theoretical point of view. It is present at the surface of most crystal alumina polymorphs, as well as at the surface of aluminum in contact to air. In fact, it is well known that metals easily oxidize in the atmosphere, forming thin oxide films on their surfaces. In the case of stainless steel, titanium, and aluminum, the passivating effect of such films is responsible for their successful utilizations as engineering materials. This surface treatment of aluminum is done mainly by anodic oxidation.[1] It has also been found that aluminum nanoclusters in low-density oxygen gas at room temperature form layers of thin alumina films.[2] Such films have a rather complex amorphous structure, and knowledge of their microscopic structure would be a very important step in the understanding of the detailed mechanism of the oxidation and passivation process. In addition, molten alumina is one of the precursors of the allotropic form $\gamma$-$Al_2O_3$, and information on the atomic level about its structure would be very useful to understand the transition from amorphous alumina towards the stable $\alpha$-$Al_2O_3$ phase.[3,4] Finally, in ceramics science, $SiO_2$-$Al_2O_3$ is one of the most important binary systems, and there is a long-standing interest in the understanding of the structure of these aluminosilicate glasses in relation to their composition and material properties.[5,6]

Amorphous $Al_2O_3$ films can be formed by anodization of aluminum in acid solution.[1] It is known that these oxide layers can be divided into two types: (i) the porous layer (''outer''), developed in acid solutions, which allows a partial solubility of $Al_2O_3$ (e.g., sulphuric acid), and (ii) the non-porous, uniform inner thin layers (''barrier''), formed in solutions that do not dissolve alumina (e.g., sodium borate). The structure of amorphous $Al_2O_3$ formed by anodization has been studied by a number of authors using different experimental techniques. Oka *et al.*[7] investigated the structure of anodic alumina films by x-ray radial distribution functions and correlations method. They prepared the anodic alumina films in sulphuric acid under two different electrolytic conditions. According to their measured spectra, the Al-O distance is 1.85 Å in both samples, whereas the Al coordination number is estimated as 4.64 and 4.81 in the films prepared using ac and dc polarizing voltages, respectively. The various peaks in the spectra were interpreted in terms of a disordered structure derived from $\gamma$-alumina, with $Al^{3+}$ ions in both tetrahedral and octahedral coordination. El-Mashri and coworkers studied amorphous alumina films by both extended x-ray absorption fine structure[8] (EXAFS) and electron extended energy loss fine structure[9] (EXELFS) techniques. They found that in the case of porous films (low density) the Al-O bond length is 1.8 Å and most Al atoms have coordination 4, whereas in the case of the nonporous films (high density), the Al-O bond length is 1.9 Å and most Al atoms are octahedrally coordinated.

Recently, Lamparter and Kniep[10] have measured the x-ray and neutron diffraction spectra of amorphous alumina films in samples prepared by anodic oxidation of aluminum foils. Together, the x-ray and neutron static diffraction spectra, they present the total pair correlation function. According to their estimates, the Al-O bond length is 1.8 Å and the Al coordination number is 4.1. Interestingly, they calculated the partial pair correlation functions from computer simulations of the structure by using the reverse Monte Carlo (RMC) method.[11] The distribution of the Al-O coordination number

 

in the RMC cluster was characterized by the frequencies 3(20%), 4(56%), and 5(22%). Thus, according this model most atoms are tetrahedrally coordinated. In the same way, the estimated Al-Al nearest-neighbor distance was 3.2 Å with a coordination of 6 and the O-O nearest-neighbor distance was 2.8 Å. Combining this result with the Al-O bond length, they concluded that the Al-O-Al bond angle between two neighbor tetrahedra is 125°. These authors also characterized the pores in the sample, giving a diameter of about 140 Å at an average distance of 340 Å.

In this contribution, we use molecular dynamics (MD) simulations in order to investigate in detail the short- and intermediate-range order of the amorphous structure as inferred from the pair distribution function, coordination number, bond angle distribution, and rings statistics. Computer simulations[12] provide a useful technique to deal with amorphous and liquid materials and to analyze their atomistic correlations. Surprisingly, as far as we know, no other simulations have been done to study the structure of amorphous alumina, although some MD simulations exist regarding structural properties of liquid alumina.[13–15] Very recently two different simulations of the oxidation of an aluminum nanocluster have been published, where some structural characterization of the amorphous surface oxides is presented.[16,17] In this sense, a detailed analysis regarding the microscopic structure of amorphous alumina would be very useful in order to compare with amorphous surface oxides as well as with previous experimental works.

This paper is organized as follows. After this introduction, in Sec. II we provide details of the MD simulation and the preparation of the amorphous state. Results for the short-range order and network topology are presented in Sec. III. A discussion of our findings is given in Sec. IV, and the conclusions are drawn in Sec. IV.

## II. COMPUTATIONAL PROCEDURE

Molecular dynamics simulations are carried out in the microcanonical ensemble ($NVE$) for $N=1800$ atoms (360 $Al_2O_3$ units), in an orthorhombic cell, using periodic boundary conditions. The system we analyze in detail was prepared at a mass density of $\rho=3.175$ g/cm$^3$ and run at $T=700$ $K$ in order to compare with a reported experiment.[10] The volume of the simulation cell was $V=26.667\times25.659\times28.045$ Å$^3$. Two additional systems, at a mass density of $\rho=3.0$ g/cm$^3$ (low density) $\rho=3.3$ g/cm$^3$ (high density) and at the same temperature, were also prepared.

### A. Interatomic potential

A most essential input in classical MD is the choice of force fields to describe the interatomic interactions. Among a number of potentials which have been developed to study $Al_2O_3$ in its different crystalline phases,[18–24] we have adopted the transferable potential of Matsui,[21] which is still simple and has been demonstrated to reproduce a number of experimental properties such as structure, density, bulk modulus, thermal expansivities, and melting temperatures among others[25–28] as well as liquid structure properties.[15] The potential employs pairwise additive interatomic terms of the form

$$V(r_{ij})=\frac{q_iq_j}{r_{ij}}-\frac{C_iC_j}{r_{ij}^6}+D(B_i+B_j)\exp\left(\frac{A_i+A_j-r_{ij}}{B_i+B_j}\right), \tag{1}$$

where the terms represent Coulomb, van der Waals, and repulsion energy, respectively. Here $r_{ij}$ is the interatomic distance between atoms $i$ and $j$, and $D$ is a standard force constant 4.184 kJ Å$^{-1}$ mol$^{-1}$. The effective charge $q$, the repulsive radius $A$, the softness parameter $B$, and the van der Waals coefficients $C$ are the energy parameters, which can be found in Refs. 15 and 21. The long-range Coulomb interactions are calculated with the standard Ewald summation technique. The equations of motion are integrated with a modification of Beeman algorithm, as is implemented in the program MOLDY,[29] using a time step $\Delta t=1\times10^{-15}$ s.

### B. Preparation of the amorphous state

The amorphous states were prepared by starting with an orthorhombic lattice corresponding to $\alpha$-$Al_2O_3$ at the density of 2.75 g/cm$^3$. We chose this initial low-density system in order to have a liquid at 5000 K at zero pressure[28] and also to avoid the unphysically attractive features of the potential at very short distance, as is discussed in Ref. 30 for this kind of potential. Thus, this initial configuration is heated to 5000 K and thermalized for over 45 000 time steps. Then, the sample is cooled to 3000 K by using a velocity scaling procedure at intervals of 10 time steps during 60 000 $\Delta t$ (i.e., at a rate of 1 K each 30 $\Delta t$). Next, the system is allowed to reach equilibrium for over 55 000 $\Delta t$ without any disturbance. With this well-equilibrated $Al_2O_3$ liquid at 3000 K we prepare three systems, with densities 3.0, 3.175, and 3.3 g/cm$^3$, by reducing simultaneously the lengths of the MD cell and the positions of all the atoms. From this stage we thermalized the systems at 3000 K for over 55 000 $\Delta t$. Finally, we lowered the temperature to 650 K during the next 650 000 time steps[31] and ran the systems for over 35 000 time steps without any disturbance. Because it is a known fact that in some cases not only the macroscopic but also the microscopic properties depend on the cooling rate,[32] other simulations were tried with different schedules and different initial configurations, but for this case no significant differences were found.

## III. RESULTS

First, we make a comparison of the calculated scattering static structure factors, both neutron, $S_N(q)$, and x ray, $S_X(q)$, with the diffraction measurements of Lamparter and Kniep.[10] Then, partial pair distribution function (PDF) $g_{\alpha\beta}$, coordination numbers, bond-angle distributions, and ring statistics are used to infer structural properties and determine the topology of our model. Atomic trajectories obtained from MD simulations are employed to calculate these kinds of positional and angular correlations by performing an average over the last 100 configurations, separated by 100 time steps.

In the case of the pair distribution function, we take the average over 2000 configurations separated by 10 time steps. All the following results correspond to a system at a density of 3.175 g/cm$^3$.

### A. Comparison with diffraction experiments

Structural correlations in amorphous $Al_2O_3$ have been studied both by neutron and x-ray diffraction techniques.[10] Our MD simulation can be compared directly to these experiments by calculating the scattering static structure factor.[33] This comparison, together with that of the pair distribution functions, constitutes a convenient test for the reliability of our model. Partial static structure factors are calculated from the Fourier transform of the corresponding partial pair distribution functions by means of

$$S_{\alpha\beta}(q)=\delta_{\alpha\beta}+4\pi\rho(c_\alpha c_\beta)^{1/2}\int_0^R r^2[g_{\alpha\beta}(r)-1]\times\frac{\sin(qr)}{qr}\,\frac{\sin(\pi r/R)}{\pi r/R}\,dr, \tag{2}$$

where $c_{\alpha(\beta)}=N_{\alpha(\beta)}/N$ is the concentration of $\alpha(\beta)$ species. The window function $\sin(\pi r/R)/(\pi r/R)$ has been introduced to reduce the termination effects resulting from the finite upper limit.[34] The cutoff length $R$ is chosen to be half the length of the simulation box.

The neutron scattering static structure factor can be obtained from the partial static structure factors by weighting them with the coherent neutron scattering lengths:

$$S_N(q)=\frac{\sum_{\alpha\beta} b_\alpha b_\beta (c_\alpha c_\beta)^{1/2}[S_{\alpha\beta}(q)-\delta_{\alpha\beta}+(c_\alpha c_\beta)^{1/2}]}{\left(\sum_\alpha b_\alpha c_\alpha\right)^2}, \tag{3}$$

where $b_\alpha$ denotes the coherent neutron scattering length of species $\alpha$. We use $b_{Al}=0.3449\times10^{-4}$ Å and $b_O=0.5805\times10^{-4}$ Å.[35]

In a similar way, the x-ray diffraction factor is calculated by the formula

$$S_X(q)=\frac{\sum_{\alpha\beta} f_\alpha(q) f_\beta(q)(c_\alpha c_\beta)^{1/2} S_{\alpha\beta}(q)}{\sum_\alpha f_\alpha^2(q) c_\alpha}, \tag{4}$$

where $f_\alpha(q)$ is the $q$-dependent x-ray form factor, given by

$$f_\alpha(q)=\sum_{i=1}^{4} a_{\alpha,i}\exp[-b_{\alpha,i}(q/4\pi)^2]+c_\alpha. \tag{5}$$

The parameters $a_{\alpha,i}$, $b_{\alpha,i}$, and $c_\alpha$ are taken from the paper of Hemmati *et al.*[36]

In Fig. 1 are shown the MD results for the neutron static structure factor $S_N(q)$ and the x-ray structure factor $S_X(q)$ together with the experimental data measured by Lamparter and Kniep.[10] In both cases the agreement with experiment

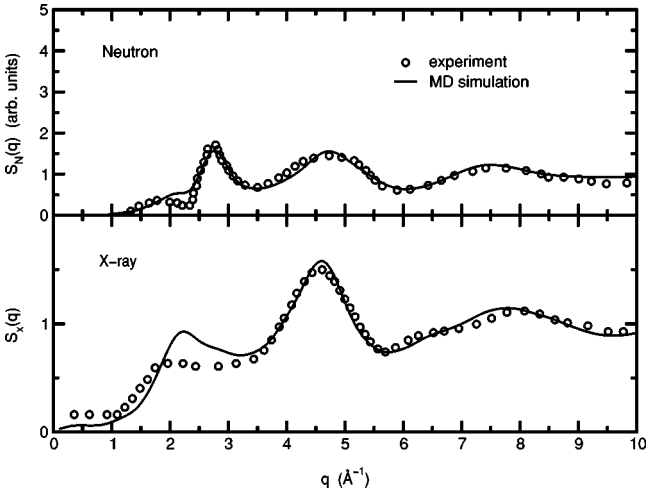


FIG. 1. Neutron and x-ray static structure function for amorphous $Al_2O_3$. Dotted line: experimental results of Lamparter and Kniep. The solid line gives the MD results.

for $q\gtrsim3$ Å$^{-1}$ is very good in terms of the shape, position, and amplitude of the peaks. For low $q$, although the simulation results do not fit completely with experimental curves, it is clear that they resemble fairly well the ''prepeak'' which is present at $q\sim2.1$ Å$^{-1}$.

The origin of the peaks in $S_N(q)$ and $S_X(q)$ can be inferred from the partial static structure factor $S_{\alpha\beta}(q)$ calculated from MD trajectories by means of Eq. (2). The results are shown in Fig. 2. It is evident that the shapes of $S_N(q)$ and $S_X(q)$ are not simply related to a single partial at any value of $q$. Instead of that, due to the particular weightings, the resulting shape involves subtle cancellations of different partials. For example, the first peak at $q\sim2.5$ Å$^{-1}$ in $S_N(q)$ involves contributions from Al-Al and O-O correlations, with a partial cancellation arising from Al-O anticorrelations, but in the case of $S_X(q)$, this peak is absent because the Al-Al and O-O partials are strongly canceled by the Al-O contribution. From the partials it is clear that the ''prepeak''

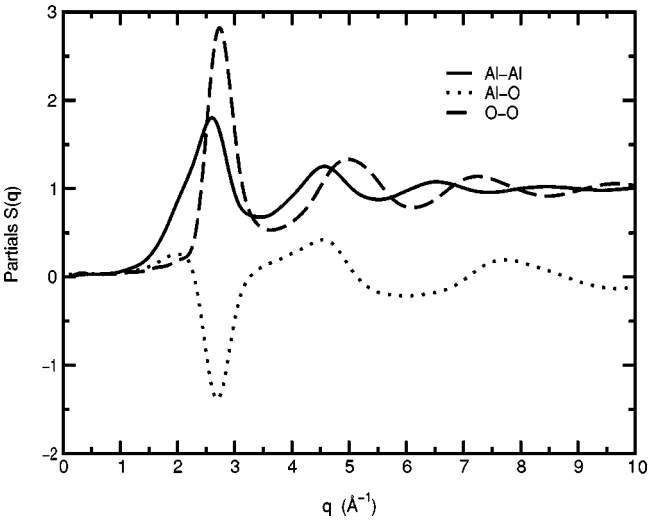


FIG. 2. Partial static structure function for amorphous $Al_2O_3$ from MD results.

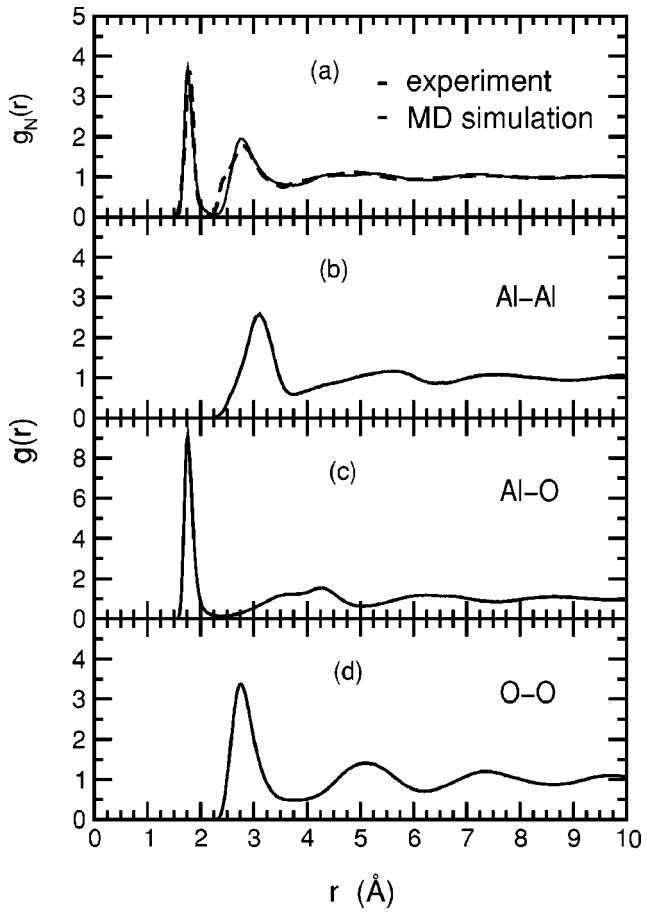


FIG. 3. Total neutron and partial pair-distribution function for amorphous $Al_2O_3$. (a) Dotted line: experimental results of Lamparter and Kniep. The solid line gives the MD results. (b) Al-Al, (c) Al-O, and (d) O-O partial pair-distribution functions.

at $q \sim 2.1$ Å$^{-1}$ arises because the low-$q$ parts of the partials are in phase, and it is not associated with a peak of any partial. In this sense, this prepeak is different from the first sharp diffraction peak (FSDP) observed, for example, in amorphous $SiO_2$, where it can be associated with a genuine peak which is presented in the three partials.[37]

### B. Short-range order

The nearest-neighborhood of an atom as defined by the shortest bond lengths and the angles between them constitutes the short-range order. It has been investigated by consideration of the partial pair-distribution functions, the coordination number, and the angle distribution. The partial pair-distribution functions $g_{\alpha\beta}(r)$ in a binary system are defined in such a way that, sitting on one atom of species $\alpha$, the probability of finding one atom of the species $\beta$ in a spherical shell between $r$ and $r+\Delta r$ is $\langle n_{\alpha,\beta}(r,r+\Delta r)\rangle = \rho_\beta 4\pi r^2 g_{\alpha,\beta}(r)\Delta r$, where $\rho_\beta = N_\beta/V$ is the number density of species $\beta$, where $N_\beta$ is the total number of atoms of species $\beta$.

In Fig. 3(a) we display the calculated total neutron-weighted pair-distribution function $g_N(r)$, defined by

$$g_N(r) = \frac{\sum_{\alpha\beta} c_\alpha b_\alpha c_\beta b_\beta g_{\alpha\beta}(r)}{\left[\sum_\alpha c_\alpha b_\alpha\right]^2}, \tag{6}$$

and compare it to the experimental one obtained by Lamparter and Kniep.[10] We can see that the agreement is not as good as in the case of $S_N(q)$ or $S_X(q)$. In spite of the coincidence in the position of the first two peaks, which are located at 1.8 Å and 2.8 Å in the experimental PDF, and at 1.76 and 2.79 Å in the computed PDF, there is a shoulder in the experimental PDF which is not represented in the simulated PDF. The curves also agree in the position of the first minima, but at distance between 4 and 6 Å they differ somewhat from each other. Note, for example, that around the second peak the experimental $g_N(r)$ has more structure than the simulated one, whereas between 4 and 5 Å the converse is true.[38] However, as we will see below, the simulated amorphous state reproduces the experimental data at short distances reasonable well.

The computed partial PDF's $g_{\text{Al-Al}}$, $g_{\text{Al-O}}$, and $g_{\text{O-O}}$ are shown in Figs. 3(b), 3(c), and 3(d), respectively. From the position of the first peak in $g_{\text{Al-Al}}$ we can infer that the Al-Al nearest-neighbor distance is $3.12 \pm 0.25$ Å. In the same way, from Fig. 3(c) we can estimate the Al-O bond length to be $1.76 \pm 0.1$ Å and the O-O bond length $2.75 \pm 0.2$ Å. The errors are inferred from the full width at half maximum (FWHM).

A useful supplementary information can be obtained by integration around the first peak in the PDF, which provides the average coordination number $n_{\alpha\beta}$,

$$n_{\alpha\beta}(R) = 4\pi\rho_\beta \int_0^R g_{\alpha\beta}(r) r^2 dr, \tag{7}$$

where $R$ is a cutoff, usually chosen as the position of the minimum after the first peak of $g_{\alpha\beta}(r)$. Within the cutoff distance $R_{\text{Al-Al}} = 3.7$, $R_{\text{Al-O}} = 2.2$, and $R_{\text{O-O}} = 3.2$ Å, the Al atom is on the average surrounded by 8.26 Al atoms and 4.25 O atoms, while the O atom is surrounded by 2.83 Al atoms and 9.47 O atoms. To get a better idea of this, we show in Fig. 4 histograms with the distribution of coordination numbers for different kinds of neighbors. We can see that the one related to the bond Al-O is very sharp: 548 (76%) of the Al atoms have tetrahedral coordination, and 158 (23%) have fivefold coordination, whereas only 12 Al atoms are sixfold coordinated and 3 Al atoms have coordination 3. In the case of oxygen atoms, most of them, 539 (78%), have coordination 3, follow by 211 (20%) O atoms with coordination 2, and only 29 (2%) with coordination 4. In contrast, the coordination number of Al-Al and O-O is rather broad, showing a maxima for 8 and 9 in Al-Al and 9 and 10 for O-O.

Further information about the local structural units is provided by the angle distribution. In Fig. 5 we display the angle distribution calculated with Al-Al, Al-O, and O-O cutoff distances of 3.7, 2.2, and 3.7 Å, respectively. From the coordination numbers we infer that the basic unit is an Al atom surrounded by four O atoms. It is well known that for an

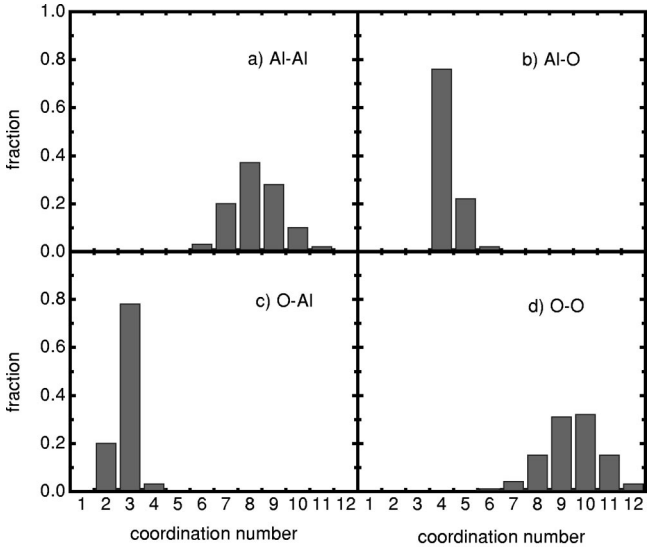


FIG. 4. Distribution of Al and O nearest-neighbor coordination in amorphous $Al_2O_3$.

ideal tetrahedron the O-Al-O bond angle is $\cos^{-1}(-1/3) = 109.47°$, the O-O-O angle is 60°, and the Al-O-O angle is 35.26°. The deviations from these values would indicate the amount of distortion with respect to an ideal tetrahedron. The O-Al-O bond angle distribution has a peak at 104°(FWHM $=30°$), O-O-O has a main peak at 60°(FWHM$=15°$), and Al-O-O present a main peak at 39°(FWHM$=15°$). Thus, combining this information with the interatomic distance and coordination numbers, we can conclude that the elementary unit of the system mainly consists of a slightly distorted $(AlO_4)^{5-}$ tetrahedron. The other basic unit which emerges from these data is a fivefold coordinated polyhedron $AlO_5$, although it is present to a much lesser extent (approximately 20%).

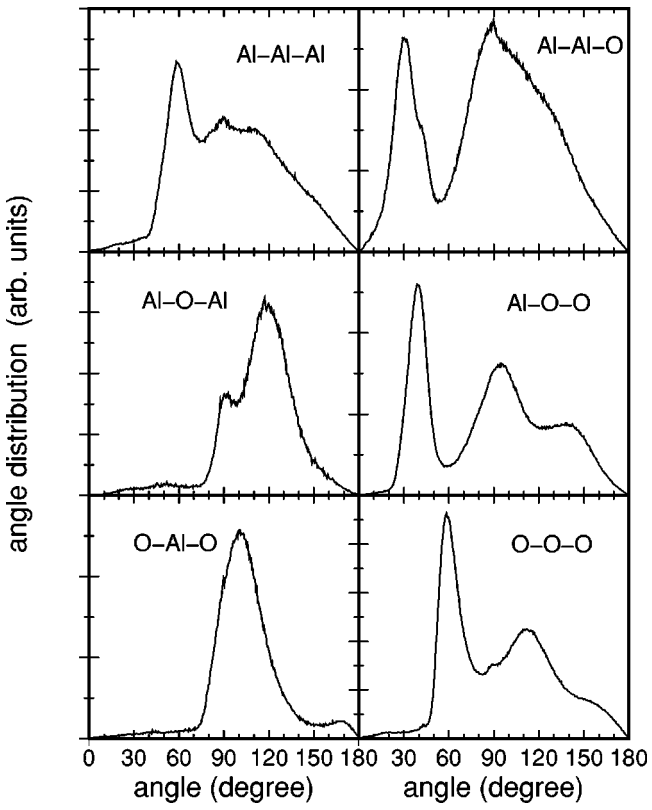


FIG. 5. Bond-angle distribution for amorphous $Al_2O_3$.

TABLE I. Short-range order in amorphous $Al_2O_3$. Comparison of the RMC model of Lamparter and Kniep to our MD simulation.

| | Lamparter and Kniep | | This work | |
|---|---|---|---|---|
| | $r_{\alpha\beta}$ | $n_{\alpha\beta}$ | $r_{\alpha\beta}$ | $n_{\alpha\beta}$ |
| Al-O | 1.8±0.21 | 4.1 | 1.76±0.1 | 4.25 |
| O-O | 2.8±0.58 | 8.5 | 2.75±0.2 | 9.47 |
| Al-Al | 3.2±0.55 | 6 | 3.12±0.25 | 8.26 |

A summary of the short-range order described here is presented in Table I, together with the results extracted from the RMC model of Lamparter and Kniep. The table shows that the differences in the interatomic distances are small, the coordination numbers being slightly larger in our work.[39] On the other hand, our results also compare well with the very recent results of Refs. 16 and 17, regarding a MD simulation of the oxidation process of an aluminum nanocluster. They found a Al-O bond length of 1.81 Å and O-Al-O angular distribution peaked at 105°. The Al coordination number ranges between 3–4 and 4–5, depending of the radius of the spherical layer around the aluminum nanocluster.

### C. Connectivity of the elementary units

The nearest-neighbor connectivity of these tetrahedra in the amorphous state is described by the Al-O-Al bond-angle distribution. It shows a small peak at 90°, and a main peak at 120°, with a FWHM of 30°. Considering this value and the remaining angle distributions one can infer that the tetrahedra are linked to each other in two principal ways, which are shown in Fig. 6. The first model, Fig. 6(a), correspond to a corner-sharing tetrahedra network and is compatible to the peak observed at $\angle$Al-O-Al$=120°$, the peak at $\angle$Al-Al-Al $=60°$, and the two peaks of the Al-Al-O distribution angle at 30° and 90°.

On the other hand, Fig. 6(b) corresponds basically to an edge-sharing polyhedra arrangement, in agreement with the small peak observed in the Al-O-Al bond angle distribution at 90° and the peak at $\angle$Al-Al-Al$=90°$ as well as the peaks shown by the Al-Al-O angle distribution at 45° and 90°. We note that if one calculates the angle distribution and coordination numbers with a smaller Al-O cutoff distance, for example 1.8 Å, the small peak at 90° in the Al-O-Al bond angle distribution and the $AlO_5$ polyhedron both disappear, given evidence for the assertion that this edge-sharing link mainly comes from the $AlO_5$ polyhedron. In this sense, we can have either two $AlO_5$ edge-sharing polyhedra or a $AlO_4$ linked by an edge to an $AlO_5$ unit.

It is not difficult to see that the remaining peaks of the Al-O-O, O-Al-O, and O-O-O angle distributions are compat-

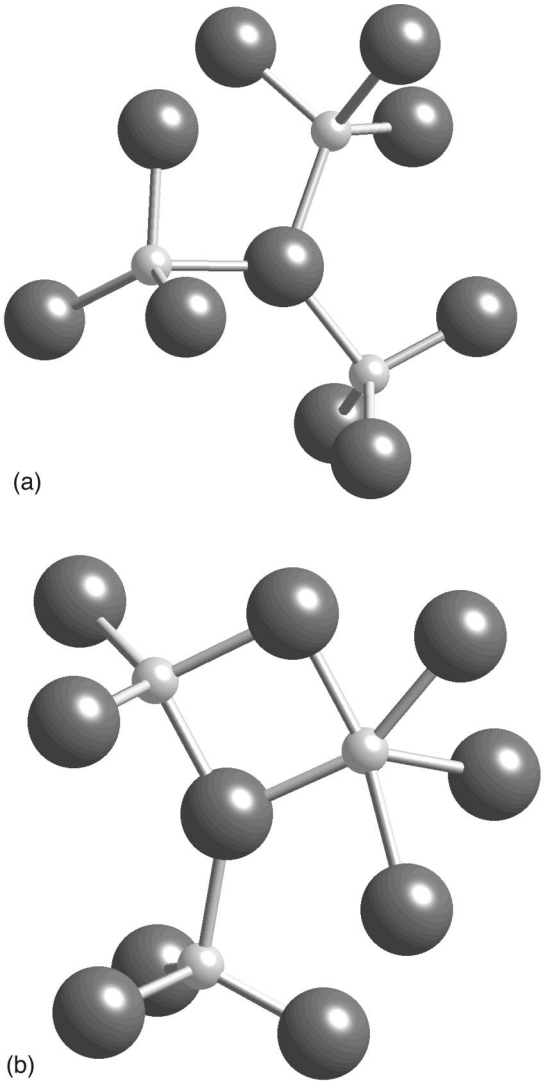


FIG. 6. Model for connectivity of the basic units in amorphous $Al_2O_3$. (a) Corner-sharing tetrahedra, (b) edge-sharing polyhedra. In both figures, the small spheres correspond to aluminum atoms and the big spheres to oxygen atoms.

ible with both models. Of course, besides these two models, there are other ways to connect the elementary units which are compatible with the calculated data. For example, 21% of oxygen atoms have coordination 2, which means that the link is only between two elementary units.

### D. Network topology

We can gain further insight into the nature of the connectivity of the elementary units beyond the nearest neighbor in terms of an *n*-fold ring analysis. An *n*-fold ring is defined as the shortest path of alternating Al-O bonds. Therefore, an *n*-fold rings consists of $2n$ alternating Al-O bonds.[40] For example, corundum has 40% of twofold and 60% of threefold rings whereas $\theta$-alumina has 23% of twofold rings, 62% of threefold rings, and 15% of fourfold rings. In Table II we display the calculated ring statistics of amorphous alumina. We found a distribution from twofold to sixfold rings,

TABLE II. Distribution of rings in amorphous $Al_2O_3$.

| Ring size ($n$) | 2 | 3 | 4 | 5 | 6 | 7 |
|---|---|---|---|---|---|---|
| Number of rings | 458 | 1683 | 2149 | 664 | 45 | 1 |

with a peak at fourfold rings (43.9%), followed by threefold rings (37.7%), fivefold-rings (12.5%), and twofold rings (9.1%). According to the angle distributions within the rings, where the twofold rings Al-O-Al and O-Al-O angle distributions have a peak at 90° and the threefold rings Al-Al-Al and O-O-O angle distributions have a peak at 60° both two- and threefold rings are planar, in contrast to four- and fivefold rings which have more complex structure. The presence of twofold rings means that the connectivity of $(AlO_4)^{5-}$ units consists not only of corner-, but also of edge- and/or face-sharing tetrahedra. However, the modest number of twofold rings suggests that most tetrahedra are linked to each other by the corner, as in Fig. 6(a), rather than by the edge and/or the face.

The ring statistics provides us with a deeper understanding of the amorphous network topology. Note that for a sample with $N$ fourfold coordinated Al atoms there are $4N \times \frac{3}{2} = 6N$ rings in the system, which corresponds to the six paths of the type O-Al-O present in the tetrahedron $AlO_4$. Similarly, in the case of $N$ fivefold and $N$ sixfold coordinated Al atoms there are $5N \times \frac{4}{2} = 10N$, and $6N \times \frac{5}{2} = 15N$ rings in the systems, respectively. Thus, knowing that we have $3\,AlO_3, 548\,AlO_4, 158\,AlO_5$, and $11\,AlO_6$ elementary units in the actual system, the total number of rings present in the system can be estimated as $3\times3+6\times548+10\times158+15\times11=5042$, i.e., very close to the actual calculated value of 5000. This give us proof of the internal consistency of our analysis.

By calculating the coordination numbers and the ring statistics with different Al-O cutoff distances, we were able to determine that the twofold rings come from $AlO_5$, as already pointed out, whereas the fivefold rings are not related to $AlO_5$ polyhedra. Moreover, we calculated approximately the number of *n*-fold rings which start either from a $AlO_4$ or a $AlO_5$ elementary unit, obtaining 833 threefold rings, 1787 fourfold rings, and 664 fivefold rings starting from a $AlO_4$ tetrahedron. This gives a total of 3284 rings, close to the estimated 3288 corresponding to the tetrahedron. In the case of the $AlO_5$ polyhedron, the corresponding total number of rings was estimated to be 1580, which can be decomposed into 458 twofold rings, 850 threefold rings, and 365 fourfold rings, giving a total of 1670 rings. The small difference with respect to the estimated value is due to the rings that start from a octahedron, which are not taken into account here.[41]

## IV. DISCUSSION

We will now comment about our findings in relation to the available experimental information, to the structural properties of the liquid, and to the different crystalline phases of alumina.

Most of the amorphous samples of the experiments we mention here has been prepared by anodic oxidation[7,8,10,42]

TABLE III. Density, coordination number, Al-O bond length, and rings statistic in terms of *n*-fold rings, for amorphous alumina (at l.d.: low density, at 3.175 g/cm$^3$, and at h.d.: high density), liquid alumina, and the crystal phases $\gamma, \theta$, and $\alpha$-$Al_2O_3$. The phase and mass density are given in the first and second columns, respectively. In the third column the coordination number of Al as well as of the O atom is given, with its respective percentage in brackets. Bond length is given in the fourth column; the upper number is the Al-O distance with higher multiplicity, and the lower number is the range of the bond length. In the last column we present the percentage of *n*-fold rings, from 2-fold to 6-fold ring.

| Phase | Density (g/cm$^3$) | Coordination number | Bond length Al-O (Å) | Ring distribution (%) 2 | 3 | 4 | 5 | 6 |
|---|---|---|---|---|---|---|---|---|
| Amorphous (l.d.) | 3.0 | Al: 3(1%),4(85%),5(13%),6(1%) O: 2(25%),3(74%),4(1%) | 1.76 (1.71–1.79) | 8.5 | 30.5 | 42 | 16.9 | 1.9 |
| Amorphous | 3.175 | Al: 4(76%),5(22%),6(2%) O: 2(20%),3(78%),4(2%) | 1.76 (1.71–1.79) | 9.1 | 33.7 | 42.9 | 13.2 | 1 |
| Amorphous (h.d.) | 3.3 | Al: 4(65%),5(31%),6(4%) O: 2(14%),3(80%),4(6%) | 1.76 (1.71–1.79) | 11.4 | 36.9 | 40.9 | 10.4 | 0.3 |
| Liquid | 3.175 | Al: 3(13%),4(66%),5(20%) O: 2(31%),3(61%),4(6%) | 1.75 (1.71–1.79) | 13 | 24.6 | 31.6 | 22.6 | 7.5 |
| $\gamma$ | 3.66 | Al: 4(30%),6(70%) O: 3(50%),4(44%),5(6%) | 1.941 (1.77–2.24) | 40 | 40 | 18.5 | 1.5 | 0 |
| $\theta$ | 3.6-3.65 | Al: 4(50%),6(50%) O: 3(66.6%),4(33.3%) | 1.904 (1.71–2.03) | 23 | 62 | 15 | 0 | 0 |
| $\alpha$ | 3.98 | Al: 6(100%) O: 4(100%) | 1.97, 1.85 | 40 | 60 | 0 | 0 | 0 |

or by rf sputter deposition.[43] In general these experiments agree in that the Al-O bond length distance is between 1.8 and 1.9 Å, and the Al coordination number has a value between 4.1 and 4.8. As regards the coordination number, it has been assumed that the elementary units of these systems consist of both ($AlO_4$) and ($AlO_6$) polyhedra, whose proportion depends on the different methods of preparation. For example, Oka *et al.*[7] quote ($AlO_4$)/($AlO_6$) ratios of 70:30 and 60:40 from films formed in sulphuric acid using ac and dc polarizing voltages, respectively. El-Mashri and co-workers[8] applied a simple model proposed by Norman *et al.*[42] to correlate the Al-O bond length with the Al coordination number. By using that model, which assumes predominantly ionic bonds and the presence of only tetra- and octahedrally coordinated Al atoms, they estimated the proportions of ($AlO_4$) and ($AlO_6$) from the reported data. Thus, the bond length $R_{\text{Al-O}}=1.85$ Å corresponds to an ($AlO_4$)/($AlO_6$) ratio of 70:30 (Ref. 42) and the Al coordination number of 4.8 corresponds to an ($AlO_4$)/($AlO_6$) ratio of 60:40 (Ref. 43). Finally, for their own experiment they found two different values. In the tartrate-formed films (the so-called nonporous films), with an Al-O bond length of 1.9 Å, the estimated proportion for the ($AlO_4$)/($AlO_6$) ratio is 20:80. In contrast, the film formed in phosphoric acid (the so-called porous films) appears to be composed of only tetrahedrally coordinated Al atoms or even lower coordination. Lamparter and Kniep,[10] after having analyzed their data by means of the RMC method, reported 20% of Al atoms with coordination 3, 56% with coordination 4 and 22% with coordination 5. The presence of a $AlO_5$ polyhedra is also reported from measurements done by Sato *et al.*[6] using NMR on an $Al_2O_3$-$SiO_2$ glass system quenched from the melt. These findings are supported by our simulation, where besides the $AlO_4$ tetrahedron (76%), an important proportion of $AlO_5$ polyhedra was found (21%).

In Table III we present a summary of our results together with the ones reported for liquid alumina[15] and structural properties of some crystalline $Al_2O_3$ polymorphs.[44–46] We note that the amorphous phase follows the same trends as liquid alumina: the Al coordination number of both phases has a peak at 4, and also the ring distribution presents a peak at the four fold ring. Because of the higher temperature, the coordination number distribution is broader in the liquid than in the amorphous phase. Since on the experimental side the coordination number and, therefore, the proportion of different polyhedra appear to be related to the density of the sample,[47] we checked our results over a density range from 3.0 to 3.3 g/cm$^3$. The small differences found in the bond length and angle distributions are reflected in the coordination number and ring distribution. It is clear from Table III that in the simulated amorphous alumina the number of overcoordinated polyhedra ($AlO_5$,$AlO_6$) increases at the same time as the number of less-coordinated polyhedra ($AlO_3$,$AlO_4$) decreases, according to the density increase from 3.0 to 3.3 g/cm$^3$. In particular, the Al coordination number changes from 4.15 in the low-density system to 4.38 in the high-density system. Therefore, we found the same behavior as reported in the experiments. Interestingly, this increase of the Al coordination number as the density increases could be related to an amorphous-amorphous phase transition,[48] which would occur at higher densities, similar to the ones observed in other tetrahedral network, such as amorphous silica[49] and germania.[50,51] The decrease of the fraction of large size rings with respect to the increase in density is

consistent with the decrease of three- and four-coordinated and the increase of five-, and six-coordinated Al atoms. Thus, highly coordinated polyhedra increase the number of small size rings and vice-versa, a trend also observed in amorphous $SiO_2$.[52,53]

It is also interesting to compare the results of our simulation to the structural properties of the crystalline phases. $Al_2O_3$ has many metastable structures, the so-called ''transition alumina,'' which are achieved by dehydration processes (thermal treatment). These processes are irreversible and all result in $\alpha$-$Al_2O_3$, a stable phase with a rhombohedral structure. Among these transition aluminas are the $\gamma$-$Al_2O_3$ (cubic spinel structure),[54], the $\delta$-$Al_2O_3$ (tetragonal structure), and the $\theta$-$Al_2O_3$ (monoclinic structure). Since our amorphous Al coordination number is close to bulk $\theta$-$Al_2O_3$, this might suggest that this crystal phase is the most likely one to obtain from the amorphous state. However, it is known that the following phase transformation to the stable $\alpha$ phase takes place:

$$\text{amorphous} \rightarrow \gamma \rightarrow \delta \rightarrow \theta \rightarrow \alpha - \mathrm{Al_2O_3}.$$

There is experimental evidence indicating that the Al atoms have a low coordination at the $\gamma$-alumina surfaces,[55] and it has been proposed that these surfaces could be considered as an amorphous like phase.[56] Our calculated coordination numbers support this conclusion, showing quite good agreement with the coordination numbers of the simulated surface from Ref. 56. It should be noted that some authors have related the amorphous state directly to $\gamma$-alumina.[57] Similarly, its short-range order has been related qualitatively to the arrangements of aluminum atoms in bohemite and pseudo-bohemite modifications of $\gamma$-alumina.[58] Also, recently it has been pointed out that different local structures of the amorphous aluminum oxide scale exist from Al nanoclusters to the bulk Al surface.[17] Thus, according to the experimental data, it seems that there are (at least) two kinds of amorphous alumina, namely, (a) one where the elementary units mainly consists of $AlO_6$ octahedra and (b) another where most of the elementary units consist of $AlO_4$ tetrahedra. Our simulations, as well as the experiments on porous samples, correspond to the latter. These two kinds of amorphous alumina would have different densities.

## V. CONCLUSIONS

In this paper we have investigated the structural properties of amorphous alumina by means of the molecular dynamics technique, using a pairwise potential. Our simulation allowed us to give a detailed account of the structural properties of amorphous alumina at the microscopic level and showed a favorable agreement with the experimental data from the work of Lamparter and Kniep,[10] especially as regards the short-range order.

The simulation shows that the amorphous state mainly consists of an arrangement of $AlO_4$ tetrahedra, linked to each other by corners, with the Al-O-Al bond-angle distribution peaked at 120°. This defines a network with a majority of three- and fourfold rings, where the threefold rings are planar, but where the fourfold rings present a more complex structure. These results show qualitative similarities to the structure of liquid alumina, both above the melting point and for the supercooled liquid. Also, we found that the calculated amorphous structure presents striking similarities to the structure of the surface of $\gamma$-alumina at room temperature. In this sense, our simulations give support to the picture that regards the surface of $\gamma$-alumina as an amorphous like phase.

The MD results for systems at three different densities, 3.0, 3.175, and 3.3 $g/cm^3$, show an increase of the coordination number of the elementary unit as the density increases. Accordingly, the number of overcoordinated polyhedra ($AlO_5$,$AlO_6$) increases. This fact suggests that the tetrahedrally and octahedrally coordinated amorphous-alumina found experimentally correspond to different densities of the samples. Similarly, it is interesting to note that the change of Al-O coordination number probably is due to an amorphous-amorphous phase transition, which is likely to take place at higher densities.

## ACKNOWLEDGMENTS

We gratefully acknowledge Ingvar Ebbsjö for providing us some of the program used to analyze the results. G.G. was partially supported by the Faculty of Science and Technology, Uppsala University, by FONDECYT (Chile) under Grant No. 1010126, and by *Iniciativa Científica Milenio* ICM P99-135-F (Chile). Part of the calculations were performed on the CRAY T3E of the National Supercomputer Center in Linköping, Sweden.

*Also at Condensed Matter Theory Group, Department of Physics, Uppsala University, Box 530, S-751 21, Uppsala, Sweden. Electronic address: ggutierr@lauca.usach.cl;
URL: http://fisica.usach. cl/~ggutierr

†Also at Applied Materials Physics, Department of Materials Science and Engineering, Royal Institute of Technology, Brinellvdgen 23, SE-100 44 Stockholm, Sweden.

[1] L. Young, *Anodic Alumina Films* (Academic Press, New York, 1961).
[2] S. Sako, K. Ohshima, and T. Fujita, J. Phys. Soc. Jpn. **59**, 662 (1990).
[3] K. Wefers and C. Misra, Alcoa Tech. Pap., No. 19 (revised), St. Louis, MO, 1987.
[4] I. Levin and D. Brandon, J. Am. Ceram. Soc. **81**, 1995 (1998).
[5] M. Morikawa, S. Miwa, M. Miyake, F. Marumo, and T. Sata, J. Am. Ceram. Soc. **65**, 78 (1982).
[6] R.K. Sato, P.F. McMillan, P. Denison, and R. Dupree, J. Phys. Chem. **96**, 4483 (1991).
[7] Y. Oka, T. Takahashi, K. Okada, and S. ichi Iwai, J. Non-Cryst. Solids **30**, 349 (1979).
[8] S.M. El-Mashri, R.G. Jones, and A.J. Forty, Philos. Mag. A **48**, 665 (1983).
[9] A.J. Bourdillon, S.M. El-Mashri, and A.J. Forty, Philos. Mag. A **49**, 341 (1984).
[10] P. Lamparter and R. Kniep, Physica B **234-236**, 405 (1997).
[11] D.A. Keen and R.L. McGreevy, Nature (London) **344**, 423 (1990).
[12] M. Allen and D. Tildesley, *Computer Simulation of Liquids* (Clarendon Press, Oxford, 1987).
[13] B.T. Poe, P.F. McMillan, B. Cote, D. Massiot, and J.P. Coutures, J. Phys. Chem. **96**, 8220 (1992).

[14] M.A. San Miguel, J. Fernández, L.J. Alvarez, and J.A. Odriozola, Phys. Rev. B **58**, 2369 (1998).
[15] G. Gutiérrez, A.B. Belonoshko, R. Ahuja, and B. Johansson, Phys. Rev. E **61**, 2723 (2000).
[16] S. Ogata and T.J. Campbell, J. Phys.: Condens. Matter **10**, 11449 (1998).
[17] T. Campbell, R.K. Kalia, A. Nakano, P. Vashishta, S. Ogata, and S. Rodgers, Phys. Rev. Lett. **82**, 4866 (1999).
[18] L.J. Alvarez, J. Fernández, M.J. Capitán, and J.A. Odriozola, Chem. Phys. Lett. **192**, 463 (1992).
[19] J.D. Gale, C.R. Catlow, and W.C. Mackrodt, Modell. Simul. Mater. Sci. Eng. **1**, 73 (1992).
[20] S. Blonski and S.H. Garofalini, Surf. Sci. **295**, 263 (1993).
[21] M. Matsui, Miner. Mag. **58A**, 571 (1994).
[22] F.H. Streitz and J.W. Mintmire, Phys. Rev. B **50**, 11996 (1994).
[23] M. Wilson, M. Exner, Y.M. Huang, and M.W. Finnis, Phys. Rev. B **54**, 15 683 (1996).
[24] C. Rambaut, H. Jobic, H. Jaffrezic, J. Kohanoff, and S. Fayeulle, J. Phys.: Condens. Matter **10**, 4221 (1998).
[25] M. Matsui, Phys. Chem. Miner. **23**, 345 (1996).
[26] M. Matsui, Geophys. Res. Lett. **23**, 395 (1996).
[27] A.B. Belonoshko, Phys. Chem. Miner. **25**, 138 (1998).
[28] R. Ahuja, A.B. Belonoshko, and B. Johansson, Phys. Rev. E **57**, 1673 (1998).
[29] K. Refson, MOLDY, release 2.13, 1998, a general-purpose molecular dynamics code. Available free for academic purpose at http://www.earth.ox.ac.uk/~keith/moldy. html
[30] J.R. Rustad, D.A. Yuen, and F.J. Spera, Phys. Rev. A **42**, 2081 (1990).
[31] The temperature was decreased linearly in time; that is, we lowered 1 K each 250 step using velocity scaling technique.
[32] K. Vollmayr, W. Kob, and K. Binder, Phys. Rev. B **54**, 15 808 (1996).
[33] Note that in our simulation the amorphous sample is prepared by a melt-and-quench technique, which differs from the reported experiments. Although it is known that when the cooling rate approaches $10^5$ K/s amorphous $Al_2O_3$ powders can be prepared, we are not aware of any experimental study about the structural properties of samples prepared in this way [C.G. Levi, V. Jayaram, J.J. Valencia, and R. Mehrabian, J. Mater. Res. **3**, 969 (1988), and references therein].
[34] E.A. Lorch, J. Phys. C **2**, 229 (1969).
[35] L. Koester, H. Rauch, M. Herkens, and K. Schröder (unpublished).
[36] M. Hemmati, M. Wilson, and P.A. Madden, J. Phys. Chem. B **103**, 4023 (1999).
[37] P. Vashishta, R.K. Kalia, J.P. Rino, and I. Ebbsjö, Phys. Rev. B **41**, 12 197 (1990).
[38] It is not easy to determine why our model fails to reproduce in detail the experimental PDF's at intermediate distances. The difference may be due to many-body effects, not accounted for the pairwise potential used here, but also it could be due to the different procedure used in the preparation of the sample (see Ref. 33).
[39] The reason for this can be found in the different cutoff used to calculate the coordination numbers and the different densities used in both simulations; the RMC model is less dense than ours and it included 3.4% of sulfur atoms.
[40] An $n$-fold ring is calculated as follows. Starting with an Al atom we locate the positions of the rest of the atoms around it, within a sphere with a cutoff radius of 2.2 Å. Then, the nearest-neighbor O atoms of the central Al are determined. Moving to one of the O atoms, we determine its nearest-neighbor Al atoms, excluding the previous Al atom. This procedure is continued until one of the atoms in the $(n+1)$th sequence corresponds to the central atom.
[41] Further conclusions from rings statistics, with details of the interatomic distance and angle distributions, will be presented elsewhere: G. Gutiérrez (unpublished).
[42] D. Norman, S. Brennan, R. Jeager, and J. Stohr, Surf. Sci. **114**, 83 (1981).
[43] T. Hanada, T. Alkawa, and N. Soga, J. Non-Cryst. Solids **50**, 397 (1982).
[44] We have calculated these numbers using the structural parameters given in Ref. 45 for $\alpha$ alumina, and in Ref. 46 for $\gamma$ and $\theta$ alumina.
[45] N. Ishizawa, T. Miyata, I. Minato, F. Marumo, and S.I. Iwai, Acta Crystallogr., Sect. B: Struct. Crystallogr. Cryst. Chem. **36**, 228 (1980).
[46] R.S. Zhou and R.L. Snyder, Acta Crystallogr., Sect. B: Struct. Sci. **47**, 617 (1991).
[47] Because samples could contain a substantial amount of pores, in general the density of Amorphous alumina is not unique, ranging from 2.95 g/cm$^3$ to 3.3 g/cm$^3$. For example, the RMC simulation of Ref. 10 was done assuming a density of 3.05g/cm$^3$ [P. Lamparter (private communication)].
[48] P.H. Poole, T. Grande, C.A. Angell, and P.F. McMillan, Science **275**, 322 (1997).
[49] M. Grimsditch, Phys. Rev. Lett. **52**, 2379 (1984).
[50] J.P. Itie, A. Polian, G. Calas, J. Petiau, A. Fontaine, and H. Tolentino, Phys. Rev. Lett. **63**, 398 (1989).
[51] K.H. Smith, E. Shero, A. Chizmeshya, and G.H. Wolf, J. Chem. Phys. **102**, 6851 (1995).
[52] R.G. Della Valle and H.C. Andersen, J. Chem. Phys. **97**, 2682 (1992).
[53] W. Jin, R.K. Kalia, P. Vashishta, and J.P. Rino, Phys. Rev. B **50**, 118 (1994).
[54] G. Gutiérrez, A. Taga, and B. Johansson, Phys. Rev. B **65**, 012101 (2002).
[55] F.R. Chen, J.G. Davis, and J.J. Fripiat, J. Catal. **133**, 263 (1992).
[56] L.J. Alvarez, L.E. León, J. Fernández, M.J. Capitán, and J.A. Odriozola, Phys. Rev. B **50**, 2561 (1994).
[57] This is the reason why this phase sometimes is referred to as $\gamma'$-alumina. See, for example, A. F. Wells, *Structural Inorganic Chemistry*, 3rd ed. (Clarendon Press, Oxford, 1962).
[58] L.A. Aleshina, E.A. Nikitina, and A.D. Fofanov, Crystallogr. Rep. **42**, 906 (1997).